Improved vascular organization enhances functional integration of engineered skeletal muscle grafts

Jacob Koffler[a,b], Keren Kaufman-Francis[a,b], Yulia Shandalov[a], Dana Egozi[c], Daria Amiad Pavlov[a], Amir Landesberg[a], and Shulamit Levenberg[a,1]

[a]Biomedical Engineering Faculty; [b]Inter-departmental Program in Biotechnology, Technion-Israel Institute of Technology, Haifa 32000, Israel; and [c]Department of Plastic and Reconstructive Surgery, Rambam Health Care Campus, Haifa 31096, Israel

Edited* by Robert Langer, Massachusetts Institute of Technology, Cambridge, MA, and approved July 25, 2011 (received for review December 9, 2010)

Severe traumatic events such as burns, and cancer therapy, often involve a significant loss of tissue, requiring surgical reconstruction by means of autologous muscle flaps. The scant availability of quality vascularized flaps and donor site morbidity often limit their use. Engineered vascularized grafts provide an alternative for this need. This work describes a first-time analysis, of the degree of in vitro vascularization and tissue organization, required to enhance the pace and efficacy of vascularized muscle graft integration in vivo. While one-day in vitro was sufficient for graft integration, a three-week culturing period, yielding semiorganized vessel structures and muscle fibers, significantly improved grafting efficacy. Implanted vessel networks were gradually replaced by host vessels, coupled with enhanced perfusion and capillary density. Upregulation of key graft angiogenic factors suggest its active role in promoting the angiogenic response. Transition from satellite cells to mature fibers was indicated by increased gene expression, increased capillary to fiber ratio, and similar morphology to normal muscle. We suggest a "relay" approach in which extended in vitro incubation, enabling the formation of a more structured vascular bed, allows for graft-host angiogenic collaboration that promotes anastomosis and vascular integration. The enhanced angiogenic response supports enhanced muscle regeneration, maturation, and integration.

angiogenesis | tissue engineering | vascular biology | regenerative medicine

Flaps serve as important elements in reconstructive surgery, however, the availability of quality autologous muscle flaps, donor site morbidity, length of procedures, and cosmetic concerns present significant limiting factors (1–6). Tissue survival is dependent on oxygen supply, which is limited to a diffusion distance of up to 300 μm from a supplying blood vessel (7, 8). Therefore, long-term survival and function is depending on rapid vascularization, which provides for the metabolic needs of the tissue. Suitable flaps lacking a sufficient blood supply may undergo necrosis (9). Engineered vascularized muscle graft may offer a clinically relevant alternative to the autologous muscle flap. However, neither the in vitro and in vivo interactions between the vasculature network and muscle fibers, nor the influence of these interactions on graft survival and postimplantation viability, have been fully elucidated (10). This work describes the dynamics of vascularized muscle graft integration in vivo. More specifically, we investigated the degrees of prevascularization and myogenesis required for improved implantation prospects. Extended incubation periods in vitro, yielded a semiorganized vascularized graft that actively contributed to angiogenesis and enhanced perfusion in vivo. In turn, accelerated host vasculature ingrowth and replacement of the preorganized vascular-like network, were observed. The improved angiogenic response influenced muscle fiber interactions with host blood vessels, along with their spatial organization and maturation. This improved integration had similar morphology to the normal muscle tissue, thus presenting new insights into the approaches of vascular and muscle integration.

Results

In Vitro Tissue Dynamics. Grafts were constructed using a triculture system of endothelial cells (ECs), myoblasts, and foreskin fibroblasts on biodegradable Surgisis scaffolds SIS is a resorbable, acellular bioscaffold, composed of extracellular matrix proteins derived from the jejunum of pigs, and has been shown to be completely replaced by the host within 90 d (11, 12). SIS contains a variety of factors including VEGF and FGF2 that are known angiogenic factors (12, 13), thus it has the potential to promote remodeling instead of a scar tissue (14). The triculture tissue proliferated and differentiated on the scaffold in vitro (Fig. 1). Within the first day of seeding, ECs had already spread from the center, where they had been seeded, and covered most of the scaffold area (Fig. 1 *A* and *B*). Following one week of incubation, ECs organized in two, spatially-distinct populations, where the lower layer included anastomosed ECs arranged in network-like structures, while the upper layer population was composed of single ECs. As the latter population gradually disappeared over the ensuing two and three weeks of incubations, most of the anastomosed structures expanded in diameter (Fig. 1*C*). At early stages of culturing, a number of anastomosed structures located along the tissue perimeter were open, yet with time, those situated at the tissue center opened as well. By three weeks postseeding, most structures were open and demonstrated vessel-like, branched networks (Fig. 1*A*). A dense and uniform myoblast population was observed, where fusion to multinucleated myofibers was already noted within one week of seeding. After three weeks in culture, straight, long fibers were observed extending across the scaffold (Fig. 1*B*). Grafts did not change in shape or size, as can be seen in Fig. 1*A*, which shows the entire surface of the scaffolds, up to the perimeters. We have shown before that myobalsts grown on poly-lactic co glycolic acid (PLGA) scaffold can exert forces that change its shape (15). However, this effect was not observed in the three-culture system, on SIS scaffolds, where most of the cells were ECs. One can affect cells and tissue organization using mechanical loading, oxygen gradient, or electrical stimulus. For example, we have shown before that different scaffold stiffness influence myoblasts viability, organization, and myotube formation (15). We did not use any of these methods, therefore the observed pattern of aligned fibers is probably the intrinsic organizing pattern of the myoblasts. ECs and myoblasts proliferated on the scaffold and began their respective differentiation processes but did not integrate to form classic, parallel and aligned fibers and vessels as in the mature muscle.

Author contributions: J.K. and S.L. designed research; J.K., K.K.-F., Y.S., D.E., D.A.P., and A.L. performed research; J.K., D.A.P., S.L., and A.L. analyzed data; and J.K. and S.L. wrote the paper.

The authors declare no conflict of interest.

*This Direct Submission article had a prearranged editor.

[1]To whom correspondence should be addressed. E-mail: Shulamit@bm.technion.ac.il.

This article contains supporting information online at www.pnas.org/lookup/suppl/doi:10.1073/pnas.1017825108/-/DCSupplemental.

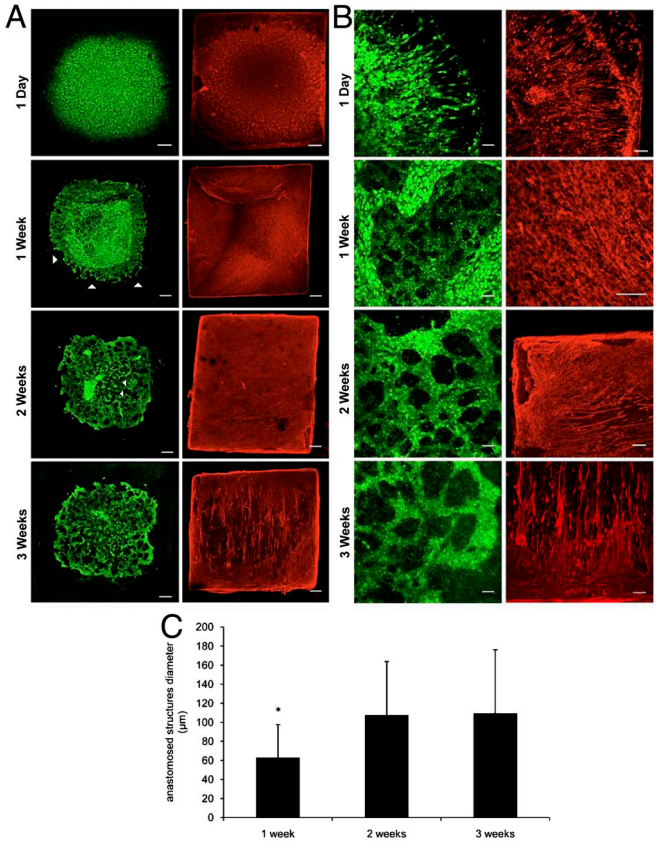

Fig. 1. In vitro grafts organization dynamics. Confocal images of triculture grafts seeded for 1 d, 1 w, 2 w, or 3 w. Green: HUVEC-GFP. Red: Desmin. (*A–B*). Visualizing tissue dynamics on the scaffold. ECs and myoblasts spread toward the perimeter within one day of cell seeding. One week later, ECs had anastomosed and created vessel-like structures, while myoblasts fused to create myofibers. Open vessel-like structures were observed along grafts perimeter (white arrow heads). Two and three weeks later, open vessel-like structures were observed at the center of the scaffold as well, demonstrating strengthening of the structures and close resemblance to natural blood vessels network. Myoblasts already populated the scaffold by day one and fused to form long fibers, as incubation times increased. Bar: A-500 μm. B-1 d, 1 w-100 μm. 2 and 3 w: 200 μm. (*C*). Diameter of anastomosed HUVEC-GFP structures. Results are presented as mean ± SD, $n = 3$, $p < 0.005$. Asterisks indicate statistical significance.

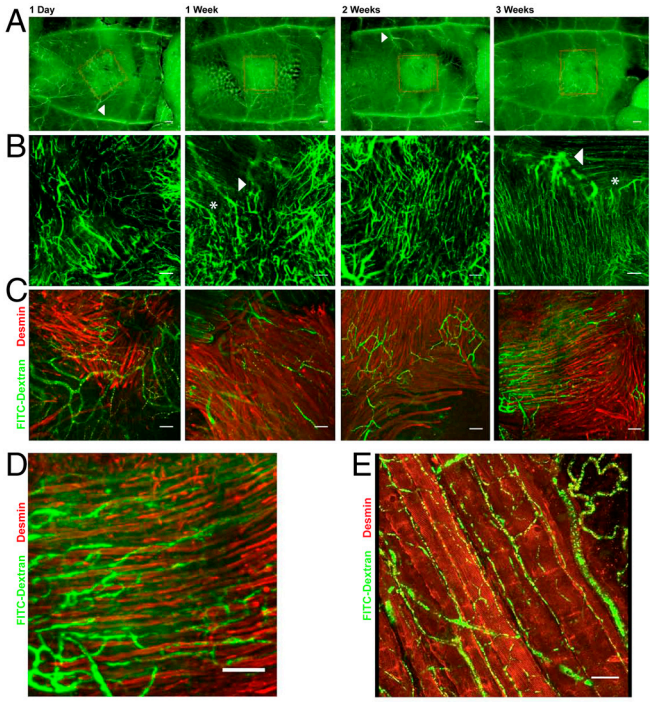

Fig. 2. Grafts integration, 14 d postimplantation. (*A*). Intravital images of the mouse abdomen wall. Grafts are marked with red frame. Grafts were connected to the host through large vessels branching from the epigastric vessels (white arrowheads). Bar-1 mm. (*B*). Confocal images of grafts. Large host vessels are visible, branching to microvessels upon reaching the graft (white arrowheads). Thin host microvessels (white asterisks) can be seen as they bend and penetrate the graft. These microvessels aligned in parallel after extended incubation times in vitro. Bar-200 μm. (*C*). Confocal images of fiber organization and integration with vessels. Green—FITC-dextran, red—Desmin. Bar-100 μm. (*D*). Higher magnification of (*C*), representing the most advanced integration of fibers and vessels. Bar-100 μm. (*E*). Confocal image of a normal abdominal muscle showing fibers in red (desmin) and blood vessels in green (FITC-dextran), aligned and parallel. Bar-50 μm. Headings represent in vitro incubation periods.

In Vivo Graft Integration. In order to assess the effects of in vitro incubation periods on tissue integration prospects in vivo, a full thickness segment of the abdominal wall of nude mice, was replaced with muscle grafts of varying degrees of maturity (3, 16). All grafts were retrieved and imaged two weeks postimplantation. This model enabled us to capture the dynamics of angiogenesis and muscle formation during integration due to host-graft interactions. Intravital microscopy and perfusion of FITC-dextran demonstrated that grafts were viable, and connected to the host via large vessels branching from the epigastric blood vessels (Fig. 2*A*, Fig. S1*A*). These large vessels branched to microvessels upon reaching the grafts. Grafts were also connected to the surrounding tissue via microvessels that bent upon reaching the grafts (Fig. 2 *A* and *B*). In vivo morphology of graft microvessels was highly dependent on the length of the graft's incubation period in vitro (Fig. 2*B*). One-day in vitro grafts exhibit loose, scattered vessel networks, while one-week in vitro grafts networks were denser. Two-week in vitro grafts demonstrated a number of aligned and paralleled vessels as can be seen in the middle of the grafts, while in three-week in vitro grafts all vessels were long, paralleled, and stretched from one side of the graft to the other. Muscle formation was evident in all grafts (Fig. 2*C*). Fibers were more ordered and closely arranged upon extended in vitro culturing times. One-day in vitro grafts present a loose organization while all the rest present dense groups of myotubes. The most mature morphology, including parallel muscle fibers and paralleled blood vessels that were also aligned together, as observed in a mature muscle tissue, was observed in three-week in vitro grafts, two weeks postimplantation (Fig. 2 *C–E*).

In order to determine the functionality of our preformed vessel network, we used muscle grafts engineered with Human Umbilical Vein Endothelial Cells (HUVEC)-GFP. At 14 d postimplantation, we perfused rhodamine-dextran and monitored graft-host integration. Surprisingly, one day of incubation in vitro was sufficient to create viable, functional HUVEC-GFP vessels that exhibited a flow of rhodamin-dextran through them (Fig. 3 *A* and *B*), despite the fact that the EC population was undifferentiated in vitro (Fig. 1*A*). With extended incubation times, fewer GFP vessels were detected, from 121.26 ± 36.85 per mm^2 in one-day grafts to 5.43 ± 2.02 per mm^2 in three-week grafts (Fig. 3 *A* and *C*).

We analyzed FITC-dextran accumulation within implanted muscular grafts as a measure of perfusion of functional vessels. Engineered vascularized grafts showed better perfusion than an empty scaffold or grafts engineered only with myoblasts (Fig. 4*A*). Among the vascular grafts, longer culture periods resulted in higher FITC signal intensity (Fig. 4*A*), meaning better perfusion of blood vessels. The amount of vessels and their diameter influence perfusion, as larger vessels can carry more FITC-dextran. Blood vessel density was increased from 161.37 ± 71.69 per mm^2 in one-day in vitro grafts to 556.2 ± 188.11 mm^2 in three-week in vitro grafts (Fig. 4*B*). It was coupled with an increase in smooth

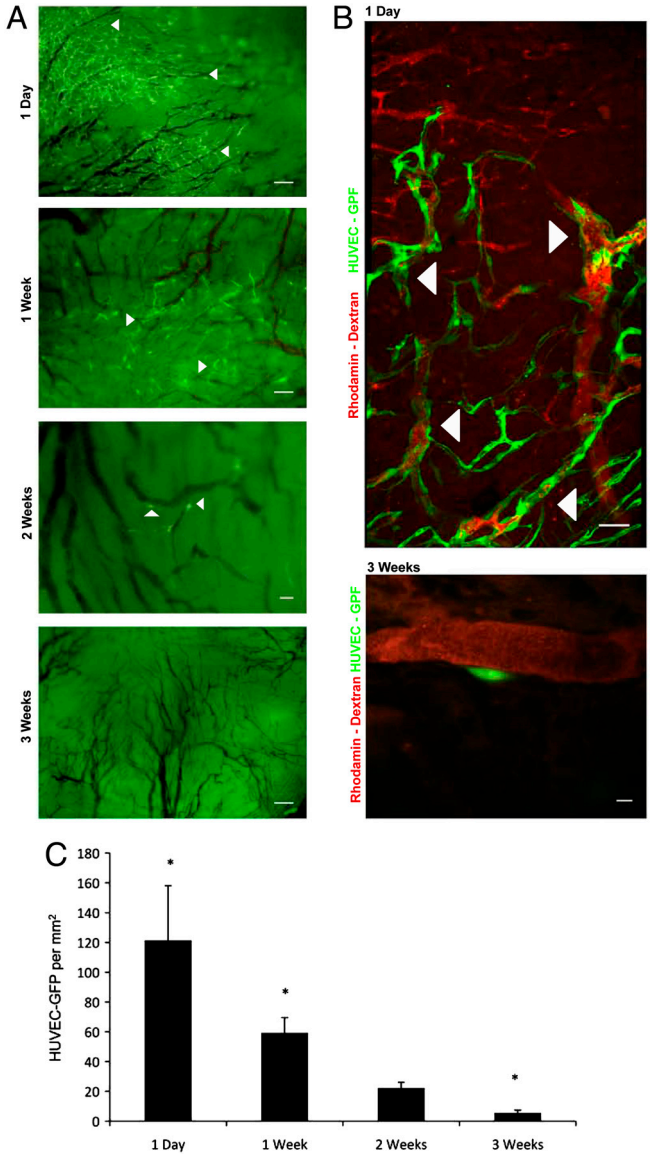

Fig. 3. Engineered vessel integration, 14 d postimplantation (*A*). Intravital images of triculture grafts including HUVEC-GFP followed by systemic perfusion of rhodamin-dextran. ECs differentiated to vessels (white arrowheads) and integrated with host vessels (black). GFP vessels were gradually decreased as in vitro incubation times extended. Bar: 1 d-200 μm, 1 w-100 μm, 2 w-50 μm, 3 week-200 μm. (*B*). Confocal image of grafts containing HUVEC-GFP perfused with rhodamin-dextran, Functional HUVEC-GFP vessels can be seen, as rho-dextran flows through them. Bar: 1 d-50 μm, 3 w-10 μm. (*C*). HUVEC-GFP density. ECs gradually disappeared with extended incubation time in vitro. $n = 5$, $p < 0.001$. Asterisks indicate statistical significance.

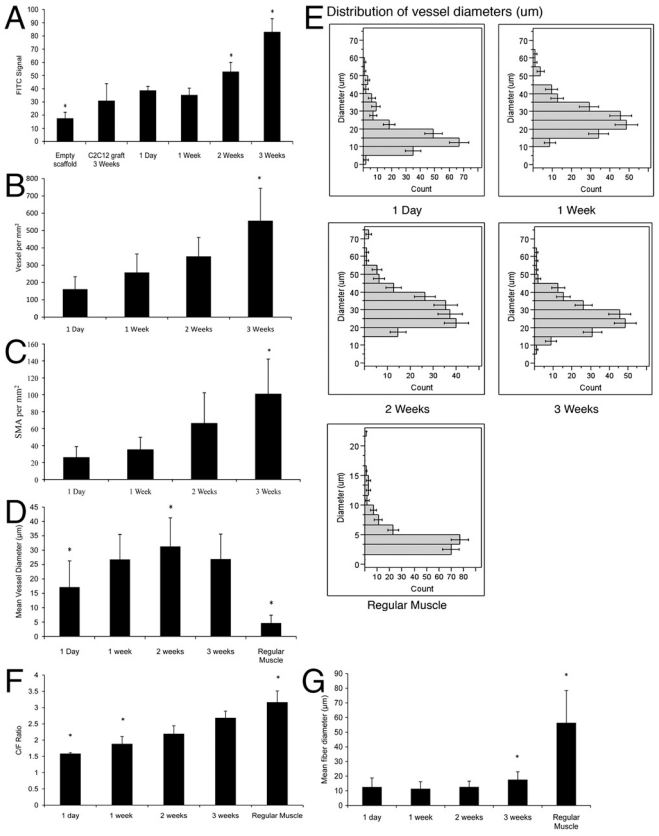

Fig. 4. Vasculogenic and myogenic parameter quantitation, 14 d postimplantation. (*A*). FITC-dextran signal in the grafts. Perfusion was better in grafts containing engineered blood vessels. Among those, perfusion improved with extended in vitro incubation periods. $n = 5$, $p < 0.001$. (*B*). Total vessel density. Three-week in vitro grafts exhibit the highest number of vessels. $n = 5$, $p < 0.01$. (*C*). Total SMA coverage. Three-week in vitro grafts exhibit the highest vessel coverage. $n = 5$, $p < 0.0001$. (*D*). Mean vessel diameter: Vessel diameters measured on grafts. In vivo vessel diameter increased over the first two weeks of grafts in vitro incubation, followed by a decrease compared to the diameter observed in adjacent normal rectus abdominis muscle. $n = 5$, $p < 0.001$. (*E*). Distribution of vessel diameters: Decrease in diameter was further demonstrated by distribution analysis, where small vessels, under 10 μm in diameter, were observed again in three-week in vitro graft. (*F*). Capillary density measured by C/F ratio: An overall increase in C/F ratios suggests progressive graft integration. $n = 5$, $p < 0.0005$. (*G*). Mean fiber diameter. $n = 5$, $p < 0.0005$. All results are presented as mean ± SD Results in (*D*) are presented with S.E. Asterisks indicate statistical significance.

muscle actin (SMA) density, from 25.75 ± 13 per mm^2 in one-day in vitro grafts to 100.7 ± 41.4 per mm^2 in three-week in vitro grafts (Fig. 4*C*, Fig. S1*B*). We also analyzed blood vessels diameter and found an increase in mean diameter from 17 ± 9 μm in one-day in vitro grafts to 31 ± 10 μm in two-week in vitro incubated grafts. However, vessel diameters decreased to 27 ± 8.7 μm in three-week in vitro grafts (Fig. 4*D*). These results suggest that the observed increased perfusion in three-week in vitro grafts was due to increased number of small blood vessels that compensated for the larger vessels observed in two-week in vitro grafts. Analysis of vessel diameter distribution revealed that microvessels under 10 μm in diameter were present at one-day in vitro grafts but not in one- and two-week in vitro grafts. However, these vessels were detected again in three-week in vitro grafts (Fig. 4*E*). We examined adjacent normal rectus abdominis muscle and found that most of the vessels were less than 10 μm in diameter (Fig. 4*E*). These results show that the vessel network, 14 d postimplantation, in three-week in vitro grafts, was the closest to the one observed in a normal mature muscle. Capillary per fiber ratio (C/F) was increased with in vitro culturing times, where the C/F ratio of three-week in vitro grafts (2.6 ± 0.2) was relatively similar to that of the normal adjacent rectus abdominis muscle (3.1 ± 0.3) (Fig. 4*F*). These results strengthen the previous observation that improved perfusion in three-week in vitro grafts was the result of higher number of microvessels. Furthermore, we observed continues expansion in muscle fiber diameter although fibers were still relatively small in comparison to normal muscle (Fig. 4*G*).

In Vivo Gene Expression. Gene expression patterns in grafts were studied in an effort to define the events controlling angiogenesis, muscle fibers development, and ECM arrangement. A sharp decrease in EC-expressed human Platelets Endothelial cell adhesion molecule (PECAM-1), progenitor EC marker (CD34), Von Willebrand factor (vWF), and VEGFR- 2 (KDR) was seen (Fig. S2*A*), correlating with the observed progressive decrease of HUVEC-

GFP in vivo as incubation times extended (Fig. 3*A*). In contrast, the human morphogenes, capillary morphogenesis genes (CMG-1, CMG-2, and CD39), angiogenic factors (VEGF-A, VEGF-B, and FGF2) and the hypoxia marker HIF1α, all critical factors in angiogenesis, vessel survival, and stabilization (17–25), were still highly expressed in three-week in vitro grafts (Fig. S2*A*). We have previously reported (16) that in the presence of ECs, foreskin fibroblasts differentiate to smooth muscle cells, colocalize with ECs, and secrete VEGF in vitro. To address this issue we labeled HFF cells with DiI (1,1'-dioctadecyl-3,3,3',3'-tetramethylindocarbocyanine perchlorate) prior to implantation and visualize them at the end point. Here we show that HFF cells survived and differentiated to smooth muscles exhibiting close interaction with blood vessels (Fig. S1*C*). This observation means that they were the source of the additional human angiogenic factors expression. Increased expression of the mouse ECs genes PECAM-1, Flk1, and thrombomodulin (THBD), supported formation and stabilization of host blood vessels (21) (Fig. S2*B*), while human ECs decreased in number (Fig. S2*A*). We observed a phenomena where low expression levels of mouse HIF1α,VEGF-A VEGF-B, FGF-2, Angoipoietin-2, CMG-1, and CMG-2 genes were observed while their human counterparts were highly expressed. (Fig. S2*B*). On the other hand it was also interesting to note that PDGF-B, which is important for vessel stabilization, was highly expressed by the host, and by the graft as well. Mouse muscle markers Pax7, c-Met, N-cam, M-cadherin, Myf5, and myogenin were upregulated (Fig. S2*C*), suggesting substantial muscle regeneration involving satellite cells activation, proliferation, differentiation, fusion to myofibers, and maturation (26–30). This expression profile was accompanied by increased expression of ECM components (Fig. S2*D*), including collagen 1, collagen 3, collagen 4, collagen 6, laminin chains α5, β1, and fibronectin. Expression of MuSK, DOK7, and laminin chains α4, α2, β2, γ1, all associated with neuro-muscular junctions (NMJ) (31–35), were not upregulated in the grafts, relatively to one-day in vitro graft. The neural marker β3-Tubulin, demonstrates that the NMJ in one-day in vitro graft was only partially developed (Fig. S1*F*), suggesting that it is not yet fully formed and organized.

In Vivo Muscle Functionality. Muscle function (contraction) was assessed by measuring the passive and active forces at 6–8 different muscle lengths for each construct, in order to obtain the force-length curves (as described in the *Materials and Methods*). The empty group showed negligible or no active stress development (Fig. 5*A*) with mean $F_a = 6.3 \pm 7.6\%$, (F_a represents the percent of active stress out of the total at $L_{\max}$). Both one-day and three-week in vitro grafts showed significantly increased active stress with mean $F_a = 34.5 \pm 20.4\%$ (Fig. 5*B*). Force-length relationship curves also stress grafts active response (Fig. 5*C*). Most triculture grafts showed an increase in force for increased muscle length (up to a certain length-$L_{\max}$), as expected from normal

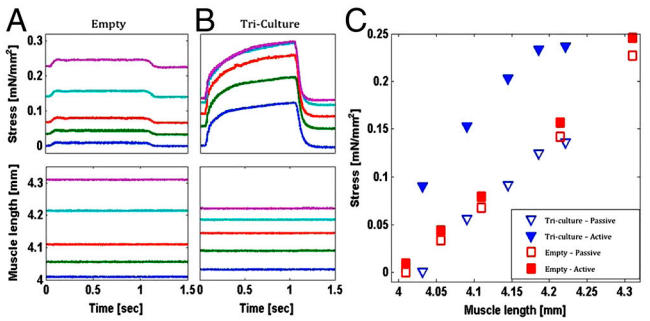

Fig. 5. In vivo functionality. (*A*). Empty constructs showed negligible active stress developed for the different lengths ($n = 4$), (*B*). Triculture grafts showed significantly increased active stress ($n = 12$). (*C*). Curvilinear force-length relationship could be observed only in triculture grafts. $p < 0.05$.

muscle tissue. Movies of graft contractions in response to stimulation are shown in Movie S1, Movie S2, and Movie S3.

Discussion

One of the major obstacles for the generation of clinically applicable tissue is to keep it viable in vivo. Successful implantation is dependent on revascularization and anastomosis of the implant with the host vasculature, otherwise ischemia and necrosis set in. This study reveals the in vivo dynamics of graft vascular integration and angiogenesis. The degree of the vascular bed organization in vitro directly influences host penetration to the graft, and the remodeling of the vascular network. Incubation of one day, where ECs were not organized yet (Fig. 1*A*), was sufficient for differentiation and anastomosis with the host (Fig. 3 *A* and *B*). This short incubation was also sufficient to yield blood perfusion that was better than grafts without ECs (Fig. 4*A*). However, in vivo perfusion and vessel density improved dramatically as incubation time lengthened to three weeks and ECs were allowed to be better organized (Fig. 1*A*, Fig. 4 *A* and *B*). This observation was followed by increased coverage with smooth muscle cells leading to stabilization and maturation of vessels (Fig 4*C*, Fig S1*B*). The improved preorganization resulted in faster replacement of graft vessels by host vessels. Fewer GFP vessels per mm^2 were detected until barely seen on three-week grafts, while total number of blood vessel per mm^2 increased (Fig. 3 *A* and *C*). This result was supported by ECs gene expression patterns that showed a reduction in human endothelial markers (Fig. 4 *A* and *B*). The newly formed vessels exhibit an increase in vessel diameter, which is a known result of ischemia (36). This increase was followed by a decrease in vessel diameter and aligned morphology. These observations outline a transformation from massive blood supply to one engaged in detailed tissue needs, providing for the progress of graft muscle maturation (Fig. 2 *C* and *D*, Fig. 4*E*). We suggest a host-graft collaboration where the angiogenic process was actively supported by key graft angiogenic factors, expressed by HFF derived smooth muscle cells. HIF1α, FGF2, and VEGF-A graft expression, along with expression of vessel stabilization factor PDGF-B by both host and graft, demonstrate that both host and graft promote implant integration (Fig. S2*B*). A recent report by Frontini, et al. showed that exogenous addition of FGF9, a factor that is upregulated by the mural cells and increase their recruitment, enhanced the angiogenic response in ischemic mouse hind limb (37). Our results enhance this finding, showing the active contribution of graft mural cells together with host stabilization of newly formed blood vessels. It has been shown that VEGF and PDGF mRNA increased expression, correlate with increased protein expression and increased vessel density, in animal and human angiogenic scenarios, such as human breast cancer, non-small-cell lung cancer, melanoma, and atherosclerotic lesions (38–42). We show that as well; a correlation between increased mRNA expression, improved vessel density, and tissue organization. Hif1α is a factor that is constitutively expressed in the cell, and degraded in normoxia. In hypoxia, Hif1α is stabilized and exerts its effect. Nevertheless, a number of groups reported the correlation between increased mRNA and increased protein expression of Hif1α that also correlated to increased vascular density. Hif1α increased levels also correlated to increased VEGF levels that, as mentioned earlier, correlate to increased vascular density (43–51). We also show this pattern in our gene expression research which correlates to the increased vascular density, as observed in the grafts. Thus, we have demonstrated that an implant can actively contribute and collaborate with the host, to promote its own integration.

Shen, et al. and Suda, et al. showed that in the bone marrow and the hippocampus, progenitor cells respond to angiogenic factors, produced by the vascular bed. These factors were shown to be essential for proliferation, differentiation, and neurogenesis of the progenitor cells (52, 53). This study shows that the preimplanted

vascular bed is essential for graft integration and organogenesis in vivo. In a regenerated muscle, once the myotubes are formed, they go through a maturation process during which they become innervated and vascularized, resulting in myofibers (10). Myofibers are then packed together by connective tissues to provide strength to the muscle. The parallel alignment of the myoblasts during fusion is the key to what gives the myofibers their ability to produce the force necessary for movement and strength (10, 54). We have brought together the vascular bed and myoblasts to improve muscle regeneration. Our grafts exhibited an increase in fiber diameter and capillary per fiber ratio in vivo (Fig. 4 *E* and *F*) as incubation time is prolonged. Further tissue maturation, similar to the normal rectus abdominis muscle, was evident by coalignment of blood vessels with muscle fibers in three-week in vitro graft (Fig. 2 *C*–*E*). This coalignment was not demonstrated in grafts engineered with only myoblasts, (Fig. S1*D*). Another control of empty SIS scaffold in vivo, showed scattered blood vessels and single, unfused, myoblasts population that resembled the single cell population observed in one-day in vitro grafts (Fig. S1*E*, Fig. 1*B*). All stages in the muscle regeneration process, from satellite cells to mature muscle, were demonstrated by real-time PCR, showing increased expression of relevant markers (Fig. S2*C*). This maturation was accompanied by an increase in the expression of ECM components (Fig. S2*D*). These components have structural roles in interstitial connective tissue and basement membrane development during angiogenesis and myogenesis, and are important to vessel function and stabilization, as well as muscle structure and force transduction (26, 32, 33, 54–56).

The functional study showed that our triculture graft contracts in vivo in response to stimulation, while the empty scaffold did not exhibit any activity. Although we could not show significant differences in activity between one-day and three-week in vitro grafts it was clear that three-week in vitro grafts were highly integrated with the host muscles, which made it very difficult to dissect the grafts based on boundary visibility (Fig. S3 *B*–*D*). The active force was about 35% of an intact muscle. This result was expected because our additional data support the fact that the grafts are not fully matured in terms of muscle fibers maturation (Fig. 4 *F*–*G*, Fig. S2*D*, Fig. S1*F*) and NMJ formation after only 14 d in vivo. Nevertheless, contraction after such a short integration period is very impressive.

The results of this study substantiate the need for vascularization and emphasize its importance for implant integration. We suggest a unique "relay" approach to engineered vascularized graft integration in vivo. The relay is the competition between the various tissue organizations states examined in vitro, to result in a more advanced maturation and integration in vivo. The more advanced organization (three-week in vitro grafts) resulted in faster anastomosis, maturation, and replacement by the host. In tissue engineering and cell therapy where endothelial cells are being used, investigators seeking to find their implanted cells or vessels in vivo, so they can show a prolonged and sustained effect over time (57). We suggest the opposite. We show that increased incubation allows for a more advanced organization that results in better perfusion increased vessel density and maturity, but gradual decrease in implanted HUVEC-GFP. Meaning once the implanted vessels anastomosed and perfused, the host is able to quickly remodel the blood vessel network to its needs. Another result is a more advanced fiber maturation and morphology where vessels and fibers are parallel and aligned, as in a mature muscle. We show the effect of ECs addition to the graft, and the resulted formation of tissue structures—the vascular tree, fibers organization, and their interaction. In addition, we suggest a collaboration in the angiogenic process, where some angiogenic factors were expressed by the graft (VEGF-A, VEGF-B, FGF2,, and HIF1α) and not by the host, while one factor (PDGF-B) was highly expressed by both. This suggested collaboration supported the observed improved integration, which results in partial functionality 14 d postimplantation, and morphology and organization that resemble the normal mature muscle organization.

Materials and Methods

Cell Culture. C_2C_{12} mouse myoblast cells [American Type Culture Collection (ATCC)] were cultured in DMEM supplemented with 20% FBS, and 2.5% Hepes buffer. Human Umbilical Vein Endothelial Cells (HUVEC, Clonetics) and HUVEC-GFP (Angio-Proteomie) were cultured in endothelial cell medium (EGM-2, EGM-MV, and their respective bullet kits, Cambrex Bio Science Walkersville, Inc.). Human foreskin fibroblasts were cultured in DMEM supplemented with 10% FBS and 1% nonessential amino acids.

Graft Preparation. Four-ply Surgisis (Cook Biotech Inc.) were rehydrated according to the manufacturer's instructions. For seeding, the desired number of cells were pooled and resuspended in 3□l culture medium. The suspension was placed on the scaffold and was allowed to be absorbed (1.5 h, 37 °C, 5% CO_2), after which 3 mL of 1:1 HUVEC-GFP:C2C12 media were added. Medium was replaced every other day. We have previously refined these conditions of media and cell numbers (16).

Fibroblast Labeling. Cells were labeled [45 min, room temperature (RT)], directly on culture plates, with 3 μL/mL Vybrant DiI (In Vitrogen) diluted in medium, and then washed three times with PBS.

Implantation of Muscle Grafts. All surgical procedures were conducted according to protocols approved by the Institutional Animal Care and Use Committee. Male, 8 w old, nude mice (Harlan Laboratories) were divided randomly to four groups, five mice per group. Mice were anesthetized using a ketamine: xylazine cocktail at a dose of 35 μL/20 g delivered with a 25-gauge needle. A small incision was made allowing access to the linea-alba and surrounding tissue, where a 3×2 mm full thickness defect segment was removed. Muscle grafts were sutured in place using four 8-0 silk sutures. All mice were monitored closely for 1–2 h to ensure full recovery from the anesthesia. Mice were anesthetized two weeks later and 10 mg/mL FITC-dextran or rhodamine-dextran (Sigma) were perfused through the tail vein. Grafts were either imaged or immediately placed into RNAlater buffer (Qiagen) until RNA extraction was performed as described below.

Tissue Processing and Immunohistochemical Staining. Whole mount: Grafts were fixed in 4% paraformaldehyde (30 min, RT) followed by extensive washing in PBS and overnight blocking (10% FBS, 0.1 g glycine, 0.1% Triton X-100, in PBS). Skeletal muscles were labeled using a goat polyclonal desmin antibody (Santa Cruz Biotechnology), smooth muscles were labeled using mouse SMA (DAKO), mouse blood vessels were labeled using FITC-ILB4 (Vector Labs), and NMJ was labeled using mouse anti βIII-tubulin (Promega). All antibodies were diluted in fresh blocking serum and incubated with samples overnight at 4 °C. Following extensive washings, donkey anti-goat, or goat anti-mouse Cy3 antibodies (Jackson ImmunoResearch Laboratories Inc.) and DAPI (Sigma) were diluted in PBS and incubated with the grafts (3 h, RT). Serial sections: Grafts were fixed for 30 min in 10% neutral buffered formalin, routinely processed, and embedded in paraffin. Serial sections (5 μm) were placed on silanized slides for immunohistochemistry as described above.

Imaging. Intravital images were captured using an Olympus fluorescent stereo microscope (SZX12). In vitro and ex-vivo images were taken with a Zeiss LSM 510 Meta Confocal microscope and Leica TCS-LSI confocal microscope. Slides were imaged using a Zeiss fluorescent microscope (Axiovert-200M).

Image Analysis. FITC intensity was measured using NIH ImageJ software, as were vessels and muscle fiber numbers and diameters. For HUVEC-GFP and vessel area calculations, images were segmented followed by quantification of signal area.

Statistical Analysis. Results were analyzed using one-tail ANOVA followed by Tukey's test using JMP 8.0 (SAS); $\alpha < 0.05$ was considered statistically significant.

RT-PCR Analysis. Total RNA was isolated using RNEasy Midi Kit (Qiagen) according to the manufacturer's muscle tissue isolation protocol. RT-PCR was performed using High Capacity cDNA Reverse Transcription Kit (Applied Biosystems). TaqMan assays were performed using custom gene expression plates and probes (Applied Biosystems), as detailed in Table S1. All human and mouse sequences were confirmed unique and noncrossreactive by

BLAST. Results were processed using DataAssist Software (Applied Biosystems) and visualized using ArrayStar software.

Force Measurements. The constructs were dissected in a bath perfused with modified Krebs-Henseleit solution containing (in mM) 143.7 Na+, 5.0 K+, 130.4 Cl–, 1.2 Mg2+, 2.26 PO4–, 19.0 HCO3–, and 10.0 glucose; pH was set at 7.40 by adjusting the flow of the gas mixture (95% O2, 5% CO2). Calcium concentration was 1.5 mM. The constructs were dissected based on the borders of the scaffold with small ends of surrounding tissue on each side for force transducer and motor arm insertion (Fig. S3*A*). The dimensions of all the constructs were fairly similar of about $4 \times 3 \times 1$ mm. The experimental bath was placed on a stage of an inverted microscope (TE300, Nikon). The bath was perfused at a constant rate, and the temperature was kept at 25 °C. The constructs were stimulated at 0.2 Hz. The stimulation amplitude was 1.5 times the stimulus threshold for maximal force production. Force was measured by a silicone strain gauge (SensorOne AE801). Muscle length was controlled by a fast servomotor (Aurora Scientific, model 308B) and monitored by a precise capacitance sensor attached to the motor axis. Tetanic stimulation (50 Hz) was performed following every regular twitch. Passive stress was calculated from baseline force at each length and active stress was calculated from the developed steady force at tetanus. Muscle length was measured from the calibrated signal of servomotor location. Muscle length and force were sampled at 5,000 Hz. Each measurement was repeated five times, and the results were averaged in order to reduce the random noise.

ACKNOWLEDGMENTS. The authors would like to thank the Technion's Lorry Lokey Infrastructure Unit and the Russell Berrie Nanotechnology Institute. This research was supported by the Israeli Ministry of Science, Levi Eshkol Scholarship, and Marie Curie International Reintegration Grants.

1. Atisha D, Alderman AK (2009) A systematic review of abdominal wall function following abdominal flaps for postmastectomy breast reconstruction. *Ann Plast Surg* 63:222–230.
2. Baechler MF, Groth AT, Nesti LJ, Martin BD (2010) Soft tissue management of war wounds to the foot and ankle. *Foot Ankle Clin* 15:113–138, http://www.ncbi.nlm.nih.gov/pubmed/19067424.
3. de Vries Reilingh TS, et al. (2007) Autologous tissue repair of large abdominal wall defects. *Brit J Surg* 94:791–803.
4. Falco EE, Roth JS, Fisher JP (2008) Skeletal muscle tissue engineering approaches to abdominal wall hernia repair. *Birth Defects Res C Embryo Today* 84:315–321, http://www.ncbi.nlm.nih.gov/pubmed?term=20189120%5Buid%5D.
5. Mertsching H, et al. (2009) Generation and transplantation of an autologous vascularized bioartificial human tissue. *Transplantation* 88:203–210.
6. Netscher DT, Baumholtz MA (2009) Chest reconstruction: I. Anterior and anterolateral chest wall and wounds affecting respiratory function. *Plast Reconstr Surg* 124:240e–252e.
7. Laschke MW, et al. (2006) Angiogenesis in tissue engineering: breathing life into constructed tissue substitutes. *Tissue Eng* 12:2093–2104.
8. Polykandriotis E, Arkudas A, Horch RE, Sturzl M, Kneser U (2007) Autonomously vascularized cellular constructs in tissue engineering: opening a new perspective for biomedical science. *J Cell Mol Med* 11:6–20.
9. Guo L, Pribaz JJ (2009) Clinical flap prefabrication. *Plast Reconstr Surg* 124:e340–350.
10. Gayraud-Morel B, Chretien F, Tajbakhsh S (2009) Skeletal muscle as a paradigm for regenerative biology and medicine. *Regen Med* 4:293–319.
11. Gilbert TW, Stewart-Akers AM, Badylak SF (2007) A quantitative method for evaluating the degradation of biologic scaffold materials. *Biomaterials* 28:147–150.
12. Woods AM, Rodenberg EJ, Hiles MC, Pavalko FM (2004) Improved biocompatibility of small intestinal submucosa (SIS) following conditioning by human endothelial cells. *Biomaterials* 25:515–525.
13. Badylak S, Liang A, Record R, Tullius R, Hodde J (1999) Endothelial cell adherence to small intestinal submucosa: an acellular bioscaffold. *Biomaterials* 20:2257–2263.
14. Hodde J (2006) Extracellular matrix as a bioactive material for soft tissue reconstruction. *ANZ J Surg* 76:1096–1100.
15. Levy-Mishali M, Zoldan J, Levenberg S (2009) Effect of scaffold stiffness on myoblast differentiation. *Tissue Eng Pt A* 15:935–944.
16. Levenberg S, et al. (2005) Engineering vascularized skeletal muscle tissue. *Nat Biotechnol* 23:879–884.
17. Goepfert C, et al. (2001) Disordered cellular migration and angiogenesis in cd39-null mice. *Circulation* 104:3109–3115.
18. Jackson SW, et al. (2007) Disordered purinergic signaling inhibits pathological angiogenesis in cd39/Entpd1-null mice. *Am J Pathol* 171:1395–1404.
19. Wagatsuma A (2007) Endogenous expression of angiogenesis-related factors in response to muscle injury. *Mol Cell Biochem* 298:151–159.
20. Lokmic Z, Mitchell GM (2008) Engineering the microcirculation. *Tissue Eng Part B-Rev* 14:87–103.
21. Carmeliet P, Conway EM (2001) Growing better blood vessels. *Nat Biotechnol* 19:1019–1020.
22. Norrby K (2006) In vivo models of angiogenesis. *J Cell Mol Med* 10:588–612.
23. Dowling O, et al. (2003) Mutations in capillary morphogenesis gene-2 result in the allelic disorders juvenile hyaline fibromatosis and infantile systemic hyalinosis. *Am J Hum Genet* 73:957–966.
24. Fedak PW (2008) Paracrine effects of cell transplantation: modifying ventricular remodeling in the failing heart. *Semin Thorac Cardiovasc Surg* 20:87–93, http://www.ncbi.nlm.nih.gov/pubmed/18707639.
25. Zhang F, et al. (2009) VEGF-B is dispensable for blood vessel growth but critical for their survival, and VEGF-B targeting inhibits pathological angiogenesis. *Proc Natl Acad Sci USA* 106:6152–6157.
26. Charge SB, Rudnicki MA (2004) Cellular and molecular regulation of muscle regeneration. *Physiol Rev* 84:209–238.
27. Le Grand F, Rudnicki MA (2007) Skeletal muscle satellite cells and adult myogenesis. *Curr Opin Cell Biol* 19:628–633.
28. Tajbakhsh S (2009) Skeletal muscle stem cells in developmental versus regenerative myogenesis. *J Intern Med* 266:372–389.
29. Tedesco FS, Dellavalle A, Diaz-Manera J, Messina G, Cossu G (2010) Repairing skeletal muscle: regenerative potential of skeletal muscle stem cells. *J Clin Invest* 120:11–19.
30. Wallace GQ, McNally EM (2009) Mechanisms of muscle degeneration, regeneration, and repair in the muscular dystrophies. *Annu Rev Physiol* 71:37–57.
31. d'Houtaud S, et al. (2009) Synapse formation and regeneration (Translated from fre). *Neurochirurgie* 55:S49–62 (in fre).
32. Durbeej M (2010) Laminins. *Cell Tissue Res* 339:259–268.
33. Grounds M (2008) Complexity of Extracellular Matrix and Skeletal Muscle Regeneration. *Skeletal Muscle Repair and Regeneration*, ed SSaT Partridge (Springer, Dordrecht, The Netherlands), pp 269–301.
34. Milholland RB, Gordon H (2007) A role for acetylcholine receptors in their own aggregation on muscle cells. *Dev Neurobiol* 67:999–1008.
35. Tzu J, Marinkovich MP (2008) Bridging structure with function: structural, regulatory, and developmental role of laminins. *Int J Biochem Cell Biol* 40:199–214.
36. Anonymous (2007) Grabb and Smith's Plastic Surgery. (Lippincott Williams and Wilkins, Philadelphia), 6th ed, p 43.
37. Frontini MJ, et al. (2011) Fibroblast growth factor 9 delivery during angiogenesis produces durable, vasoresponsive microvessels wrapped by smooth muscle cells. *Nat Biotechnol* 29:421–427.
38. Battegay EJ, Rupp J, Iruela-Arispe L, Sage EH, Pech M (1994) PDGF-BB modulates endothelial proliferation and angiogenesis in vitro via PDGF beta-receptors. *J Cell Biol* 125:917–928.
39. Forsberg K, Valyi-Nagy I, Heldin CH, Herlyn M, Westermark B (1993) Platelet-derived growth factor (PDGF) in oncogenesis: development of a vascular connective tissue stroma in xenotransplanted human melanoma producing PDGF-BB. *Proc Natl Acad Sci USA* 90:393–397.
40. Li J, et al. (1995) Induction of vascular endothelial growth factor gene expression by interleukin-1 beta in rat aortic smooth muscle cells. *J Biol Chem* 270:308–312.
41. Scott PA, et al. (1998) Differential expression of vascular endothelial growth factor mRNA vs protein isoform expression in human breast cancer and relationship to eIF-4E. *Br J Cancer* 77:2120–2128.
42. Yuan A, et al. (2000) Correlation of total VEGF mRNA and protein expression with histologic type, tumor angiogenesis, patient survival and timing of relapse in non-small-cell lung cancer. *Int J Cancer* 89:475–483.
43. Fu D, Dai A, Hu R, Chen Y, Zhu L (2008) Expression and role of factor inhibiting hypoxia-inducible factor-1 in pulmonary arteries of rat with hypoxia-induced hypertension. *Acta Biochim Biophys Sin* 40:883–892.
44. Furlan D, et al. (2007) Up-regulation and stabilization of HIF-1alpha in colorectal carcinomas. *Surg Oncol* 16:S25–27.
45. Jiang H, Feng Y (2006) Hypoxia-inducible factor 1alpha (HIF-1alpha) correlated with tumor growth and apoptosis in ovarian cancer. *Int J Gynecol Cancer* 16:405–412.
46. Lee S, Garner EI, Welch WR, Berkowitz RS, Mok SC (2007) Over-expression of hypoxia-inducible factor 1 alpha in ovarian clear cell carcinoma. *Gynecol Oncol* 106:311–317.
47. Liang B, et al. (2010) Correlation of hypoxia-inducible factor 1alpha with angiogenesis in liver tumors after transcatheter arterial embolization in an animal model. *Cardiovasc Inter Rad* 33:806–812.
48. Mori R, et al. (2010) The relationship between proangiogenic gene expression levels in prostate cancer and their prognostic value for clinical outcomes. *Prostate* 70:1692–1700.
49. Qiu MZ, et al. (2011) Expressions of hypoxia-inducible factor-1alpha and hexokinase-II in gastric adenocarcinoma: the impact on prognosis and correlation to clinicopathologic features. *Tumour Biol* 32:159–166.
50. Wang W, et al. (2009) Expression and correlation of hypoxia-inducible factor-1alpha, vascular endothelial growth factor and microvessel density in experimental rat hepatocarcinogenesis. *J Int Med Res* 37:417–425.
51. Yohena T, et al. (2009) Upregulation of hypoxia-inducible factor-1alpha mRNA and its clinical significance in non-small cell lung cancer. *J Thorac Oncol* 4:284–290.
52. Shen Q, et al. (2004) Endothelial cells stimulate self-renewal and expand neurogenesis of neural stem cells. *Science* 304:1338–1340.
53. Suda T, Arai F, Hirao A (2005) Hematopoietic stem cells and their niche. *Trends Immunol* 26:426–433.
54. Grounds MD, Sorokin L, White J (2005) Strength at the extracellular matrix-muscle interface. *Scand J Med Sci Spor* 15:381–391.
55. Francis ME, Uriel S, Brey EM (2008) Endothelial cell-matrix interactions in neovascularization. *Tissue Eng Part B-Rev* 14:19–32.
56. Jain RK (2003) Molecular regulation of vessel maturation. *Nat Med* 9:685–693.
57. Koike N, et al. (2004) Tissue engineering: creation of long-lasting blood vessels. *Nature* 428:138–139.